AIIM

Association for Information and Image Management

1100 Wayne Avenue, Suite 1100
Silver Spring, Maryland 20910

301/587-8202

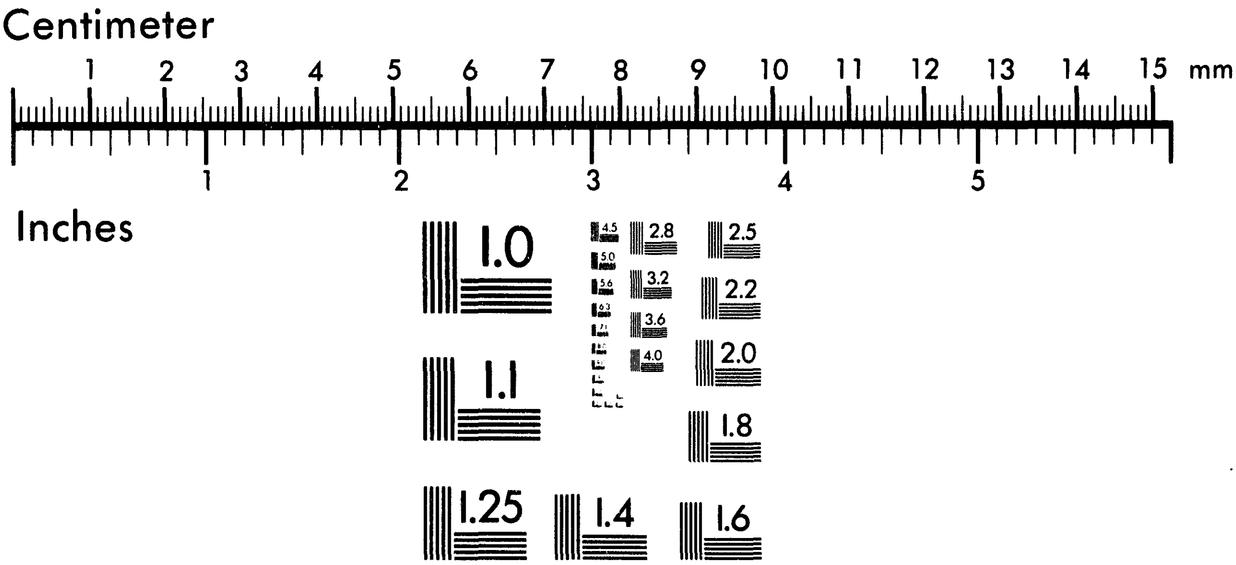

MANUFACTURED TO AIIM STANDARDS
BY APPLIED IMAGE, INC.

1 of 1

MATERIALS AND MECHANISMS OF HIGH TEMPERATURE LITHIUM SULFIDE BATTERIES

T. D. Kaun, M. C. Hash, G. L. Henriksen, A. N. Jansen, and D. R. Vissers

Argonne National Laboratory
Chemical Technology Division
Electrochemical Technology Program
9700 South Cass Avenue
Argonne, IL 60439

May, 1994

To be published in the Proceedings of the II Chilean Symposium, Santiago, Chile, May 24-27, 1994

TABLE OF CONTENTS

LIST OF FIGURES

LIST OF FIGURES (cont'd)

LIST OF TABLES

MATERIALS AND MECHANISMS OF HIGH TEMPERATURE LITHIUM SULFIDE BATTERIES

T. D. Kaun, M. C. Hash, G. L. Henriksen, A. N. Jansen, and D. R. Vissers

Argonne National Laboratory
Chemical Technology Division
Electrochemical Technology Program
9700 South Cass Avenue
Argonne, IL 60439

Abstract

New materials have encouraged development of bipolar Li-Al/FeS_2 batteries for electric vehicle (EV) applications. Current technology employs a two-phase Li-alloy negative electrode low-melting, LiCl-rich LiCl-LiBr-KBr molten salt electrolyte, and either an FeS or an upper-plateau (U.P.) FeS_2 positive electrode. These components are assembled in a sealed bipolar battery configuration. Use of the two-phase Li-alloy (α + β Li-Al and $Li_5Al_5Fe_2$) negative electrode provides *in situ* overcharge tolerance that renders the bipolar design viable. Employing LiCl-rich LiCl-LiBr-KBr electrolyte in "electrolyte-starved" cells achieves low-burdened cells, that possess low area-specific impedance; comparable to that of flooded cells using LiCl-LiBr-KBr eutectic electrolyte. The combination of dense U.P. FeS_2 electrodes and low-melting electrolyte produces a stable and reversible couple, achieving over 1000 cycle life in flooded cells, with high power capabilities. In addition, a family of stable sulfide ceramic/sealant materials was developed that produce high-strength bonds between a variety of metals and ceramics, which renders lithium/iron sulfide bipolar stacks practical. Bipolar Li-Al/FeS_2 cells and four-cell stacks using these seals are being built and tested in the 13 cm diameter size for EV applications. To date, Li-Al/FeS_2 cells have attained 400 W/kg power at 80% DOD and 180 Wh/kg energy at the 30 W/kg rate. When cell performance characteristics are used to model full-scale EV and hybrid vehicle (HV) batteries, they are projected to meet or exceed the performance requirements for a large variety of EV and HV applications. Efficient production and application of Li-alloys and Li-salt electrolyte are critical to approaching battery cost objectives.

1.0 INTRODUCTION

Since the mid-1980's, Argonne National Laboratory (ANL) has been conducting a low-level parallel research project on Li-Al/FeS_2 and Li-Al/FeS cells [1,2,3] for electric vehicles. Several major technical developments on this project have produced a shift in emphasis, away from prismatic Li-Al/LiCl-KCl/FeS cells and batteries, to bipolar Li-Al/LiCl-LiBr-KBr/FeS_2 and Li-Al/LiCl-LiBr-

KBr/FeS cells and batteries that operate at 400-450°C. The Li-Al/FeS_2 technology being pursued involves discharge on the upper voltage plateau (U.P.) of a dense FeS_2 cathode:

$$2Li\text{-}Al + FeS_2 < \text{---} > Li_2FeS_2 + 2Al \quad (1)$$

The theoretical specific energy for this reaction is 480 Wh/kg.

Developments in materials and electrochemical mechanisms for molten-salt batteries have provided significant advances to Li/FeS_2 battery performance. Stable electrochemistry and metal/ceramic seal technology[1] have encouraged a sealed bipolar battery design (Fig. 1). The bipolar battery is series-connected cells which depends upon no open circuit failures for stable operation. Additionally, overcharge tolerance of cells by a lithium-shuttle mechanism has promoted development of high voltage battery operation in which cell charge equalization can be accomplished by trickle-charging the entire battery.

Two major advantages of the bipolar design over other design configurations are higher performance and lower material costs. Higher performance results from reducing the internal impedance, thereby increasing specific power, and reducing the weight and volume of nonactive materials, and therefore increasing specific energy. Also, reducing the non-active/active material ratio reduces the materials' costs on a dollars/kWh basis.

This paper will review these technical achievements in light of materials developed. High temperature lithium battery technology promises outstanding performance, as well as a cost-effective approach for the demanding electric car application. As indicated, new materials are leading the way for meeting the ambitious cost objectives, $100/kWh. More efficient production of lithium alloys and lithium salts will improve commercial prospects for materials suppliers and profit margins for battery manufacturers. Currently, Argonne has teamed with SAFT America (Cockeysville, MD) who will commercialize the bipolar Li/FeS_2 battery for electric cars.

2.0 THE Li/FeS_2 CELL

As described in Section 1.0, bipolar lithium/sulfide batteries utilize a lithium-alloy negative electrode, a molten salt electrolyte and either an FeS or FeS_2 positive electrode. Unlike earlier cells that used the LiCl-KCl eutectic (m.p. 356°C) electrolyte and discharged the FeS_2 to Li_2S and Fe, these cells use the LiCl-LiBr-KBr electrolyte (m.p. ~320°C) and the FeS_2 electrode is discharged only to Li_2FeS_2. These type cells are referred to as U.P. Li-Al/FeS_2 cells, since they use only the upper voltage plateau of the FeS_2 half-cell couple: $FeS_2 + 2Li^+ + 2e^- \rightarrow Li_2FeS_2$.

Although theoretical specific energies of the U.P. FeS_2 cell and FeS cells are similar (460 to 475 Wh/kg), the U.P. FeS_2 cell has specific energy and power capabilities (200 Wh/kg and 200 W/kg) which are almost double those of the FeS cell. The higher voltage, as shown in Fig. 2, and lower impedance of the U.P. FeS_2 electrode are combined with 50% greater utilization of theoretical capacity. The energy density of the U.P. FeS_2 electrode is about 1.90 Wh/cm^3, compared to about 1.05 Wh/cm^3 for the FeS electrode. In addition, cell power (V^2/R) for the U.P. FeS_2 cell is about double that of the FeS cell. Voltage for the U.P. FeS_2 cell is about 35% higher, and cell impedance at 80% depth of discharge (DOD) is about 80% of the FeS cell impedance.

Therefore, the U.P. FeS cell can achieve a much higher fraction of theoretical energy than the FeS cell based on similar supporting structure weight and cell volume.

The positive FeS_2 electrodes are fabricated by cold-pressing mixed powders of metal sulfides and electrolyte salts. The FeS_2 electrode typically contains 10-15 mol% CoS_2 or NiS_2 as a conductivity enhancement additive. FeS_2 electrodes are fabricated in a 90% state of charge, with Li_2S as a source of lithium to form Li-Al_2Fe_5 at the negative electrode. Electrode performance is linked to a balance of ionic and electronic conductivity of the porous-bed electrode. According to the Bruggeman equation[4], $Km = (1 - f)^{3/2}$, where Km is the bed/dense body conductivity ratio and f is the electrolyte fraction. Thus, increasing electrode loading density from 32 to 50 vol % doubles the electronic conductivity of the FeS_2 electrode[5]. Accordingly, the best performing U.P. FeS_2 electrodes have a theoretical capacity density of 2.4 Ah cm^{-3} (50 vol%).

Initially, electrodes were evaluated in 3 cm diameter electrolyte-starved cells employing the LiCl rich LiCl-LiBr-KBr electrolyte at 425°C. These cells incorporated 30 wt% MgO pressed-powder separators with thicknesses of 2 mm. Similarly, the Li-Al/FeS_2 cell exhibited an U.P. FeS_2 electrode utilization of about 90% of the 625 mAh theoretical capacity at about 100 mA cm^{-2}, as shown in Fig. 3. At 200 mA cm^{-2}, the U.P. FeS_2 utilization was about 70%. Also, the combined use of U.P. FeS_2 electrodes and the LiCl-LiBr-KBr electrolyte at 425°C has extended the cycle life of this technology to more than 1000 cycles in flooded cells[6].

The overpotential required to charge the FeS_2 electrode is believed to be one of the key factors in the observed limited cycle life of the Li-Alloy/FeS_2 two-plateau cells (<150 cycles) that use the LiCl-KCl eutectic electrolyte. The soluble active positive electrode species that are formed at these high overvoltages [7,8] tend to migrate to the separator where iron and lithium sulfide are precipitated. The consequence of this is an increase in cell impedance and a significant and rapid capacity decline.

To circumvent this capacity decline problem, Kaun [9] shifted to a lithium-ion rich electrolyte (25 mol% LiCl - 37 mol% LiBr - 38 mol% KBr), which has a very broad liquidus region, and operated the cell only on the upper plateau, i.e., $FeS_2 \leftrightarrow Li_2FeS_2$ (see Fig. 4).

Cell testing has shown that these cells exhibit high specific energy and power and stable capacity with extended cycling. The reason these cells have excellent capacity retention, compared to earlier cells, is not completely understood, but it probably results from a combination of effects. First, the cells are operated at a lower temperature, reducing the solubility of any harmful soluble species framed. Secondly, the broad liquidus region of the LiCl-LiBr-KBr electrolyte (Fig. 4) permits significant electrolyte composition changes (Li^+/K^+ ratio of 1.25-1.81) without salt precipitation, thus, one can operate the FeS_2 electrode with active material loading densities of 50 vol% solids in the fully charged state, which also reduces transport of any soluble transition metal species from the electrode. Thirdly, on the upper plateau, the FeS_2 electrode is reported[10] to be more reversible in the LiCl-rich LiCl-LiBr-KBr electrolyte than in the LiCl-KCl electrolyte, where the higher Li^+ ion content of the electrolyte tends to eliminate K^+ ion-containing electrode phases, such as $LiK_6Fe_{24}S_{26}Cl$ and $KFeS_2$, which tend to interfere with the kinetics of FeS_2 formation.

Li-alloy/FeS_2 cell electrochemistry has been modified as we sought to replace the BN felt separator with an MgO powder separator, which has the potential for lower costs and greater

thermodynamic stability in overcharge-tolerant U.P. FeS_2 cells. However, the MgO powder separator, since it is not physically stable under flooded electrolyte conditions, must be operated in an "electrolyte-starved" cell configuration. In our efforts to develop an electrolyte-starved, overcharge-tolerant cell, we fabricated and tested LiAl + 10 % $Li_5Al_5Fe_2$/U.P. FeS_2 cells (22.5-Ah capacity) with LiCl-LiBr-KBr electrolyte and 100-cm^2 MgO powder separators. These cells demonstrated performance comparable to that of the flooded cell with BN felt separator. To increase the ionic conductivity of the electrolyte-starved cell, which is normally about 30% lower than that of the flooded cell, the electrolyte composition was shifted off-eutectic to a LiCl-rich composition (in mol%, 34 LiCl-32.5 LiBr-33.5 KBr), which has a 25% higher ionic conductivity than that of the eutectic at 425°C[11]. This higher ionic electrolyte conductivity approximately compensates for the reduced electrolyte content of the electrolyte-starved cell. Therefore, the area specific impedance (ASI_i) of the electrolyte-starved monopolar cells (1.1 Ω cm^2) is comparable to that of the flooded cell (1.1 Ω cm^2). The capacity utilization of the electrolyte cells after more than 50 cycles (>85% at discharge current density of 50 mA/cm^2) is now slightly greater than that of the flooded cell.

The effect of conductive additives[9] to the positive electrode (NiS_2, CoS_2) was studied to evaluate the improvement in electrode performance in the LiCl-rich electrolyte. In cells containing the new electrolyte and no electrode additive, about 85% utilization of theoretical FeS_2 capacity was seen at the 50 mA/cm^2 discharge rate, and, in general, utilization was 10% lower than that seen in similar cells containing an additive. In addition, the impedance of an U.P. FeS_2 electrode without additive was about 10-15% higher (1.1 Ω cm^2) than that of an electrode containing 10 mol % NiS_2 (0.9-1.0 Ω cm^2). The increased impedance here appears to be electronic rather than ionic in nature; thus, the ASI at 45 ms (the electronic impedance) is about 0.6 Ω cm^2 for electrode with no additive, compared to 0.5 Ω cm^2 for the electrodes with 10 mol % NiS_2 additive. The ASI vs. depth of discharge (DOD) curve for U.P. FeS_2 electrodes with or without additive remains flat during the bulk of the discharge, however. The electrolyte-starved U.P. FeS_2 electrode without conductive additives may have adequate performance for some applications, but noticeable improvement results from just 10 mol % NiS_2 additive. Thus, we have attained satisfactory performance without use of the expensive CoS_2 additive.

The negative Li-Al electrode is normally not discharged into the single-phase Al region, because the cell voltage would be greatly reduced[12]. (See Fig. 5). Thus, during cycling the electrode reaction is

$$\beta\text{-Li-Al} \leftrightarrow \text{Li} + \alpha\text{-Al} + e^- \qquad (2)$$

The theoretical capacity of the (α + β)-Li-Al containing 47 at. % lithium is 0.74 Ah/g, but increases as the lithium content is increased to 50 or 55 at % Li[13].

As the Li-Al/FeS_2 cell technology moved from the prismatic cell configuration to the high-performance bipolar cell configuration, it became necessary to develop overcharge tolerance for the cells. This overcharge tolerance is needed to enable the state-of-charge of all cells in a bipolar stack to be equalized. Under normal operating conditions, the cells tend to become unbalanced (see Section 6.0). The basis of the developed technique is to increase the lithium activity in the negative electrode sufficiently during cell overcharge so that a significantly higher level of self-discharge is created in the cells that have reached the fully charged state[14]. To

avoid having the Li-Al alloy material in the negative electrode becoming liquid at these high lithium activities (< 50 mV vs. lithium) approximately 10 mol Al_5Fe_2 is added to the negative electrode.

As one charges a cell into the overcharge region the following electrochemical and chemical reactions occur:

Electrochemical Reactions (3)

$$15Li^+ + 15\bar{e} + 3Al_5Fe_2 \xrightarrow{\text{cathode}} 3Li_5Al_5Fe_2$$

$$5Li_3Fe_2S_4 \xrightarrow{\text{anode}} 10FeS_2 + 15Li^+ + 15\bar{e}$$

Chemical Reactions (4)

$$Li_5Al_5Fe_2 \rightleftharpoons Li_{dissolved}$$

$$3Li_{dissolved} + 2FeS_2 \rightarrow Li_3Fe_2S_4$$

The chemical reactions give rise to a controllable rate of self-discharge caused by the presence of dissolved lithium metal in the electrolyte. Further details of this overcharge tolerance mechanism are given in Sections 3.0 and 4.0.

3.0 LITHIUM-ALLOY ELECTRODES

A variety of lithium alloys have been tested for use in secondary Li-alloy/iron sulfide cells, including those shown in Table 1. This table illustrates the effects of the density and usable capacity of the alloys upon the effective capacity density of the electrode. The effective capacity density, as defined for this table, involves the total volume of the alloys, but not the volume of the electrolyte associated with the electrode. Most of the lithium/sulfide cells use Li-Al negative electrodes. In early studies of the Li-Al/FeS cell, the rate of capacity decline was unacceptably high (as high as 0.25% per cycle). Metallographic examinations identified agglomeration of the porous Li-Al electrode as the main cause of this rapid capacity decline[15]. These electrodes were cold-pressed to high loading densities and discharged to about 85% lithium utilization. Under these conditions, the electrodes sintered at the center to produce dense structures with high aluminum content, which did not react readily with lithium ions on charge.

Methods of circumventing electrode sintering during operation have included preparation by slurry formation or the use of additives to cold-pressed pellets. Electrodes made by forming a slurry of the Li-Al powders in an organic solvent (which was later removed by evacuation) produced electrodes having longer lives than cold-pressed pellets without additives. However, the use of carbon or MgO powder additives in cold-pressed pellets produced electrodes with battery cycle-life stability better than those produced by the slurry forming method (without additives). Cold-pressing of Li alloy with MgO powder and electrolyte salt has become the preferred method for Li alloy electrode fabrication. Capacity decline of the Li-Al electrode was reduced to about 0.02% per cycle. Cells of this type having about 300-Ah capacity had a mean time to failure of about 1000 cycles.

The lithium-silicon alloy electrode has a higher theoretical specific energy than Li-Al because silicon is light and will accept several atoms of lithium per atom of silicon[16-18]. However, the use of silicon as an alloying agent for lithium is not as advantageous as it would first appear[13].

Table 1. Capacity Densities of Secondary Li Electrodes

Composition	Density (g/cm^3)	Theoretical capacity (Ah/cm^3)	Usable capacity[a] (% of theoretical capacity)	Effective capacity density (Ah/cm^3)
$Li_{3.2}Si$	1.05	1.80	65	1.17
Li-Al (50 atom % Li)	1.75	1.39	82	1.14
Li-Al (53 atom % Li)	1.65	1.47	85	1.25
$Li_5Al_5Fe_2$	2.77	1.26	85	1.07
$Li_{2.21}CaSi_2$	1.41	0.84	95	0.80
50 atm % Li-Al + 50 atom % $Li_{3.2}Si$	1.28	1.44	80	1.15
88 atom % Li-Al + 12 atom % $Li_{3.2}Si$	1.66	1.44	80	1.15

[a]Electrode capacity having lithium activity of ≤ 0.45 V vs. lithium.

First, at least one of the lithiums (about 25-30 mol%) is unusable because it is released at too low an operating cell voltage. This additional lithium increases the volume of the electrode, decreasing the effective capacity density compared to that of Li-Al (Table 1) and results in a cost penalty for the expensive unused lithium. Second, the rate of reaction for the Li-Si electrode is lower (particularly on the lowest-voltage plateau) than that for Li-Al. This results in a higher specific impedance for the Li-Si electrode than for the Li-Al electrode during a 15-s high-rate discharge, such as would be needed for acceleration of an electric vehicle. Finally, silicon is corrosive to the steel current collector; nickel may not be acceptable for Li-Si electrodes, whereas

steel current collectors show negligible corrosion in contact with Li-Al. Improved designs may result in the Li-Si alloy being favored over Li-Al, but in current designs, the Li-Al alloy appears to have a slight overall advantage in specific energy, power, and cost.

Ternary lithium-alloys have been under development to improve upon the Li-Al and Li-Si electrode properties. Also as in Table 1, the Li-Al Si electrodes have effective capacity densities that are similar to that of Li-Al about 1.15 Ah/cm^3. Generally, higher lithium activity than is afforded with Li-Al at the beginning of discharge is exchanged for lower lithium activity at 80% depth of discharge. Even though the $Li_5Al_5Fe_2$ alloy[19] has significantly higher density, 2.65 g/cm^3, it possesses higher Li-activity (-260 mV vs LiAl) through 80% DOD. Effective capacity density at 1.07 Ah/cm^3 is similar to Li-Al. Another concern is introduced for electrode development, that of the lithium-shuttle mechanism (LSM). As discussed in detail later, the Li-alloy electrodes of our bipolar cells make use of the LSM by using a two phase alloy of Li-Al and Li-Al_5Fe_2. The high lithium activity, that is developed at the end of charge, provides overcharge tolerance and cell balancing. Recently, Lagos, et al.[20] described a $Li_{2.2}CaSi_2$ lithium alloy for molten-salt electrolyte. This lithium-alloy electrode has a very favorable lithium potential of -90 to -140mV vs a $\alpha + \beta$ LiAl reference. Its capacity density is about 25% lower than the other alloys, but continued development could improve this feature. Although, the LiCaSi electrode needs to prove its cycle life, it represents an approach for increasing cell performance along with efficient use of lithium. An objective of continued research on lithium-alloy electrodes is to increase the effective capacity density and to increase the lithium activity and cell voltage, especially at 80% depth of discharge. A further objective is to avoid the inclusion of unavailable lithium, which is quite considerable for the Li-Si electrode as noted above.

An Li-alloy electrode exhibiting bimodal lithium activity[21] has been developed to provide overcharge capacity , as well as overcharge tolerance, using the LSM. Figure 6 shows the potential vs. capacity for a 25-Ah LiAl electrode in which 10% of its lithium capacity overcharge capacity has been substituted by $Li_5Al_5Fe_2$. This two-phase Li-alloy electrode has a decreased potential of -190 to -140 mV over its last 10% of charge. The open-circuit potentials may be 10 mV more negative under trickle charge rates. A cell using this Li-alloy electrode should exhibit increased self-discharge related to the high lithium activity, which imparts overcharge tolerance. A coulometric assessment of a Li-alloy/FeS_2 cell with the two-phase Li-alloy electrode reveals the LSM rate change. The cell (1.8 mm thick separator) is charged to voltage cutoff (2.05 V) and discharged in Cycle 1. Its coulombic efficiency at 425°C indicates a 0.15 mA/cm^2 self-discharge rate. Cycle 2 includes a 3-h trickle charge at 3.5 mA/cm^2 near full-charge state. The reduced coulombic efficiency indicates a 3.0 mA/cm^2 self-discharge rate (LSM) during the trickle-charge period. As the cell reaches full charge, at greater than 2.00 V, the two-phase Li-alloy electrode has transitioned to a 200 mV more negative potential. In confirmation of the increased LSM rate during trickle-charge, both cycles 1 and 2 yield the same discharge capacity.

Figure 7 plots the voltage during the charge half-cycle, along with the associated self-discharge rate for an overcharge-tolerant FeS^2 cell operated at 415°C in the upper-voltage plateau (U.P.). The bimodal self-discharge rate of the cell is coupled with a transition in its voltage/capacity curve due to the two-phase Li-alloy electrode. As the cell begins its transition into the overcharge capacity state, the self-discharge rate increases in a stepwise fashion by 20-fold, to about 2.5 mA/cm^2. In the overcharge state, the cell exhibits voltage and self-discharge characteristics relative to the $Li_5Al_5Fe_2$ constituent of the lithium electrode versus the U.P. FeS_2 electrode. Consistent with a typical 2.00 V charge cutoff, the bimodal character of the two-phase

Li-alloy electrode yields a cell with a unique combination of overcharge capacity and overcharge tolerance.

4.0 LITHIUM MOLTEN SALT ELECTROLYTES

Three lithium-ion-containing molten salts have been employed in lithium/sulfide battery development: LiCl-KCl, LiCl-LiBr-KBr, and LiF-LiCl-LiBr[22]. We have recently determined conductivities as a function of temperature for their eutectic compositions using the *AC* impedance technique. The results are plotted in Fig. 8. Each of these molten salts has unique properties that affect cell development. The LiCl-KCl eutectic has a 354°C melting point, while cells are operated at 450°C, where the conductivity is 1.4 S cm^{-1} [23]. Although the LiCl-KCl electrolyte was the baseline electrolyte for primary thermal batteries and secondary batteries, it is being replaced by the three-component salts. The LiF-LiCl-LiBr (all Li-ion electrolyte) has the highest conductivity about 3.0 S cm^{-1} at 450°C[11]. On the other hand, the LiCl-LiBr-KBr electrolyte, with its low melting point of 320°C and broad liquidus region, allowing large Li/K ion ratio deviations from that of the eutectic, provides a stable operating environment at 400°C for the FeS_2 electrode[3]. It has a conductivity of 1.3 S cm^{-1} at 450°C. The Li^+ and K^+ ion activities of these molten salts regulate solubilities of charge/electrode discharge products and electrode kinetics. As will be discussed later, self-discharge rates, cell performance, and cycle-life stability strongly depend upon the electrolyte properties.

Use of LiCl-LiBr-KBr electrolyte allows Li/FeS cell operation at considerably lower temperatures (400-425°C) than with other electrolytes (LiCl-KCl or LiF-LiCl-LiBr). In general, Li/FeS cells with LiF LiCl-LiBr are operated at 475°C, where corrosion reactions are, more likely to limit cycle life. Also, thermal management of the Li/FeS battery operated at 475°C requires an active heating and cooling system, whereas at 425°C greater temperature fluctuations can be tolerated to ease requirements of the thermal management system.

A variation of this electrolyte, an LiCl-rich composition, was identified as the electrolyte of choice for use in "electrolyte-starved" cells (i.e., cells that contain only a limited quantity of electrolyte in the pores of the separator). The LiCl-rich composition (in mol%, 34 LiCl-32.5 LiBr-33.5 KBr) possesses a 25% higher ionic conductivity (1.7 S cm^{-1}) than the LiCl-LiBr-KBr eutectic at 425°C (Fig. 8). This higher conductivity allows these electrolyte-starved cells to operate with a cell impedance, ASI_t comparable to that of flooded cells that employ the eutectic electrolyte[11].

As discussed briefly in Section 3.0, a "lithium shuttle" mechanism was developed to provide lithium/sulfide cells with an overcharge tolerance capability[21] [24-25]. This is accomplished by forming a different lithium alloy in the negative electrode, as the cell reaches the overcharged state. This alloy possesses a higher lithium activity than the standard $\alpha + \beta$ Li-Al alloy, thereby significantly increasing the concentration of lithium metal dissolved in the electrolyte. Dissolved lithium is free to diffuse across the electrolyte/separator and react chemically at the positive electrode in a self-charge reaction. The higher dissolved lithium concentration produces a higher-self-discharge rate and allows electrochemical charging of the cell to proceed at a rate equivalent to the self discharge rate without causing any net change in the state-of-charge of the cell. The ultimate lithium shuttle mechanism (LSM) rate is controlled by the lithium activity of the overcharge alloy, the electrolyte composition, the operating temperature, and the structure and

thickness of the separator. Figure 9 illustrates the effects of electrolyte composition and temperature on the "lithium shuttle" rate for a given alloy and separator design. The rates are fit to Arrhenius expressions for the three electrolyte compositions shown. These rate expressions agree well with available physical data for lithium solubility, including dimerization of lithium for the respective molten-salt compositions. That is, Li_2^+ would form in all-Li (LiF-LiCl-LiBr) electrolyte, whereas LiK^+ would for in the K^+ containing molten salts (LiCl-KCl and LiCl-LiBr-KBr). In general, the electrolyte composition establishes a level of lithium solubility to enable the LSM[21].

5.0 LITHIUM COMPATIBLE STRUCTURAL MATERIALS

Despite the fact that lithium/sulfide cells and batteries employ active and corrosive chemicals at 400°C, they do not present any unmanageable materials compatibility problems. The relatively high sulfur activity of FeS_2 limits the type of materials that can be used as electrically conductive current collectors (bipolar plates) in the Li-Al/FeS_2 battery. Also, for both Li-Al/FeS and Li-Al/FeS_2 batteries, the lithium activity associated with overcharge tolerant Li-alloy electrodes limits the type of electrical-insulating materials that can be used as the separator. Furthermore, development of a practical bipolar battery design introduces the need for a peripheral seal material that provides a leak-free seal between metals and ceramics and is tolerant of thermal cycling. This section discusses separator, bipolar plate, and seal materials that have been found to work well for bipolar lithium/metal sulfide cells and stacks.

5.1 Separators

Magnesia powder was selected for the separator because it is more widely available and less costly[26-29]. Also, it has a greater chemical stability than BN fiber in contact with lithium at high activity. A MgO powder separator with very high surface area and 70-80 vol % molten salt provides a separator with plastic-like properties. However, cells having MgO powder separators must be operated in an electrolyte-starved state to avoid formation of a low viscosity suspension of MgO in the electrolyte, which would allow the electrodes to touch and form a short circuit. The MgO powder separator is fabricated as a cold-pressed plaque from finely ground particles of electrolyte salt and high surface area MgO. These plaques have been made in disks up to 13 cm diameter and 12 x 17 cm sheets of 1-2 mm thickness. Generally, the separator is physically supported by perforated metal sheets. Cost considerations have driven separator development toward the use of MgO, possibly combined with other materials to enhance the resilience and tortuosity of the separator for particle retention, rather than the use of perforated metal sheets.

Others have investigated porous rigid plaques (eg. AlN)[30], as replacements for the electrolyte-starved MgO powder separator. Reduced electrolyte fractions, on the order of 50%, require that these new separators be much thinner (0.5-0.8 mm) to compensate for their lower ionic conductivity. A further challenge is to develop fracture toughness for the thin, porous, ceramic plates.

5.2 Bipolar Plate

The higher sulfur and chlorine activities encountered in cells with FeS_2 electrodes require current collector materials having higher corrosion resistance. In most Li-Al/FeS_2 cells,

the bipolar plate material for the FeS_2 electrode has been molybdenum. Other materials considered include carbon, tungsten, titanium nitride, and titanium carbide, all of which need further development. The molybdenum oxidation potential is 2.4 V vs. Li-Al, which is 0.35 V above the normal charge voltage cutoff of 2.05 V. The corrosion rate was found to be sufficiently low, such that a 0.025 mm thick molybdenum layer on a metallic surface would provide a 10-year corrosion life [31].

A bipolar plate of TiN coated steel is an attractive alternative to molybdenum for the positive current collector in the Li/FeS_2 bipolar cell. This material earlier was evaluated in a 3 cm bipolar Li/FeS_2 cell. The cell was operated 40 cycles (200 h) at 415°C with more than 97% coulombic efficiency at current densities up to 100 mA cm^{-2}. Upper-plateau FeS_2 cell capacity utilization was about 85% at 50 mA cm^{-2}. The cell demonstrated a tolerance for thermal cycles. These results indicate that pinhole-free coatings were achieved, because coatings with pinholes typically exhibit rapid performance degradation. This coating was produced using high-temperature multilayer chemical vapor deposition (Richter Precision, Pennsylvania). Post-test metallographic examination confirmed the stability of the TiN coated steel collector. In subsequent tests of TiN coated steel in a 13-cm diameter cell, embrittlement of the steel substrate led to coating failure. However, a TiN-coated Hastalloy B current collector, which successfully operated over 750 h at 425°C in a 13 cm diameter cell, further validated the stability of the TiN coating. Future development of this approach will pursue specifications for the steel that will avoid substrate embrittlement.

5.3 Bipolar Peripheral Seal

A key to the successful development of lithium/sulfide bipolar batteries is a metal/ceramic bonded peripheral seal for each cell[32,33]. The development of corrosion-resistant sulfide sealants[34] at ANL led to metal/ceramic bonds that are an order of magnitude stronger than those obtainable with commercially-available sealants for service over 300°C. This peripheral seal aids in achieving long life by eliminating electrolyte leakage from and between cells of the bipolar stack [35].

Requirements for the Li-Al/FeS_2 seal are that they:

- possess properties of an electrical insulator;
- provide strong bonds to metals and ceramics;
- maintain bonds during cool-down from formation at 1100°C and during thermal cycles between room temperature and 450°.
- remain stable to electrode active materials and electrolyte over the same temperature range;
- provide gas-tight seals.

The sulfide ceramic sealants appear to meet all these requirements. They can be specially formulated to accommodate differences in thermal expansion between steel, molybdenum and ceramics by forming "graded" ceramic seals. They exhibit greater than 95% coverage and wetting angles that approach 0° for both steel and molybdenum. Additionally, we have achieved a six fold increase in fracture strength of the sulfide structural ceramic through changes in its composition.

The sulfide ceramics[35] are based on non-transition metal sulfides (rather than conventional oxides, nitrides or borides). The sulfide ceramics provide a unique combination of properties (Table 2), for advanced component development. Specifically, a group of new sulfide compounds was discovered, which include silicon, aluminum, lithium calcium, sodium and other non-transition metals. These sulfide compounds are characterized by relatively low melting temperatures 700-1100°C and have excellent chemical stability similar to compounds which generally melt at 2000°C or greater. Inherent chemical stability of crystalline (rather than glassy) sulfide ceramics encourages high temperature application (400-1000°C). A sulfide ceramic based on $CaAl_2S_4$, for example, has unique properties offering prospects for a variety of new engineering applications. As an "enabling" material, sulfide ceramics display high-strength bonding to other materials, engineered properties and inherent stability to specific highly corrosive environments. A significant application of sulfide ceramic, thus far, has been to couple together metal components in large diameter electrically-insulating configuration for service within severely-corrosive, high temperature environments, Fig. 1.

Table 2. Sulfide Ceramic Materials Properties

1.	A ceramic insulator with low fusion temperatures (850°C - 1050°C).
2.	Chemical stability to alkali metals in molten halides at 400°C to 500°C.
3.	Engineered thermal expansion properties of composite materials, 5 to 15 x 10^{-6}/°C.
4.	Fused ceramic wets a broad range of metals, ceramics, and graphite.
5.	Excellent bonding to metals by self fluxing.

As bonding and sealing agents, the sulfide ceramics form a strong reaction bond with a broad range of metal components. The sulfide ceramic melts, aggressively wets, and attacks the metal surface to strongly bond as interlocking fingers of metal and ceramic, Fig. 10. In joining metals to ceramics, they produce bonds up to 20 times stronger than those of other bonding agents. Sulfide ceramics could replace welding for joining materials that are difficult to weld, such as graphite, molybdenum, and tungsten. Using these sulfide-based materials in metal/ceramic seals eliminates the need for diffusion bonding under high temperature and pressure. These ceramics can produce strong bonds in materials with coefficients of thermal expansion that differ significantly (such as, graphite coupled to steel).

As a structural ceramic component, the sulfide ceramics are a composite of a fusible material enveloping solid aggregate, such as oxides, nitrides and other sulfides. The aggregates dictate physical properties such as coefficient of thermal expansion (CTE), ceramic toughness, and fusion temperature flow properties. Aggregate materials are also used to change the electrical properties of the ceramic. Additionally, by choosing aggregates having the appropriate properties, structural ceramics can be engineered to have a CTE that reduces stress at metal/ceramic interfaces. As in Fig.11, sulfide ceramic compositions have CTE that range from 6.5 to 15 x 10^{-6}/°C.

at metal/ceramic interfaces. As in Fig.11, sulfide ceramic compositions have CTE that range from 6.5 to 15 x 10^{-6}/°C.

Effective modulus of rupture (MOR) was determined for selected sulfide ceramics using a 3-point bend method. These MOR's are on the order of 10,000 to 15,000 psi, (100 MPa) which is approximately that of sintered MgO [36]. In our seal fabrication, these sulfide ceramics 60 mil thick (1.5 mm thick) are laminated with either 5 mil thick (0.126 mm) molybdenum or steel. The MOR of the laminated metal/ceramic/metal component increases by at least 50% over the sulfide ceramic itself. Annealing of the metal/ceramic bonded laminate will occur at a 400-450°C operating temperature to further increase laminated component MOR.

As shown in Table 3, the standard sulfide sealant produces strong bonds. In many cases, the substrate ruptured before the ceramic bond. In forming a bond to molybdenum, the bound strength is increased more than seven-fold by producing an intermetallic surface layer on the molybdenum prior to bond formation. In comparison to commercially available, high temperature bonding agents (e.g. borosilicate glass, Aremco products), the standard $CaAl_2S_4$ sealant exhibits bond strengths approximately ten times greater. Also, the chemical stability of these sealants makes them ideally suited for high temperature battery applications. Additionally, as a result of their excellent wetting properties, bond formation does not rely on a thermal/compression process; thus, the bonding is not unidirectional.

We have successfully fabricated over four dozen 13 cm I.D. peripheral seals and evaluated them in bipolar lithium/sulfide cells. The bipolar Li/FeS_2 cell uses a steel/ceramic/molybdenum peripheral seal. Coated-steel materials or Grafoil have been investigated as replacements for molybdenum as the positive current collector. The unique properties of the sulfide ceramics and sealants enable formation of stress absorbing metal/ceramic seals using a variety of materials. Large-diameter components possessing different coefficients of thermal expansion (e.g., molybdenum/steel) have been bonded together using a single-composition ceramic ring.

Table 3. Tensile Strength of Bonded Surfaces

Bond Couple	Surface Area (cm^2)	Fracture Load ($kg\ cm^{-2}$)
Mo/standard sealant/Mo	2.0	3.2
Mo/standard sealant/Mo (Mo intermetallic used)	0.5	23.0
Mo/borosilicate glass/Mo	0.5	3.47
Al_2O_3/standard sealant/Al_2O_3	0.72	19.76
MgO/standard sealant/MgO	0.4	52.87
Steel/standard sealant/MgO	0.48	>35.6*
TiN coated steel/standard sealant/TiN coated steel	0.5	>16.7*
Steel/Aremco 565/MgO	1.5	1.4+

The initial work to establish long-term stability and reproducibility of seals was conducted using approximately 2.5 cm I.D. components. We prepared six bipolar seals using similar ceramic compositions and processing methods. One seal was leak-checked at a vacuum of 100 μm Hg, the limit of our test fixture. Another seal was used to build a sealed bipolar Li/FeS_2 cell to establish thermal-cycle (25 to 425°C) stability. This cell operated for more than 400 charge/discharge cycles and 2000 h with less than 10% capacity loss. The remaining four seals were used to fabricate sealed bipolar Li/FeS_2 cells which were assembled into a four cell stack.

This four cell stack operated for more than 500 cycles (2500 h) with more than 98% coulombic efficiency[37] to demonstrate seal stability. Three of the four original cells were employed throughout the 500 cycles, while one initially weak cell was replaced at 150 cycles. Bipolar stack capacity (0.45 Ah) was at least 90% that of individual cells. The stack operated at 425°C using 4 h charge and 2 h discharge rates, with charge and discharge cutoff voltages of 8.2 and 5.4 V, respectively. The average stack discharge voltage of approximately 6.5 V greatly exceeded the decomposition voltage of the molten salt electrolyte, 3.2 V. Thus, extended operation of this stack verified the ability of our seals to maintain individual cell isolation. This initial bipolar stack was assembled from four individual cells stacked with nickel felt pads and voltage leads between the cells. The stack impedance was 0.7 ohm cm^2 of cell area, which is within 130% that of individual cells, in spite of the added intercell contact resistance. Improvement resulting from stack integration indicate that stack impedance should be less than that of the cells, because of greater uniformity in intercell contact. The voltage and capacity of individual cells were sufficiently well matched that charge equalization was needed only every 20 cycles. Charge equalization was achieved without electronic equipment, using our chemical overcharge tolerance capability, as shown in Fig. 12. The stack was effectively charge equalized when all the cells had reached the overcharge capacity state.

Our bipolar cell and stack scale-up efforts involve the setup of equipment capable of handling the fabrication of 13 cm. I.D. metal/ceramic seals. The fabrication facility incorporates a 200 ton hydraulic press (Tee Tool, Joplin. Mo), a large 1100°C seal processing oven, ceramic powder preparation equipment, welding equipment, and bipolar stack test stations, all contained within a high-purity argon glovebox. This equipment permits the development and evaluation of alternative designs and processing methods. In our current bipolar seal design, the metal current collector components are attached to each other with a 2 mm thick 13 cm I.D. ceramic ring. This ceramic ring is formed from pressed powders of chalcogenide ceramic materials.

The seal components are designed for a simple stacking assembly method. The metal components are each bonded to the ceramic ring (an electrical insulator) via parallel horizontal surfaces. The metal components are custom designed and fabricated by stamping 5 mil sheet metal (Meyer Tool, Oak Lawn, IL). The seal is formed in a single thermal processing step performed at 1100°C. Subsequent thermal cycle testing is performed between 25 and 400°C to evaluate seal mechanical durability. Metal/ceramic interfaces prepared in this manner have remained crack free after thermal cycling. It is anticipated that further evolution of the seal design will lead to improvements in fabrication and durability. The sulfide ceramics can be engineered to meet new seal design objectives.

One objective of our seal development effort for bipolar Li/FeS_2 is to incorporate a molybdenum bipolar plate in such a way that the stack does not require a difficult Mo-Mo weld during final assembly. As described elsewhere[36], the preferred seal configuration of steel

ring/ceramic/Mo cup/steel ring has been successfully fabricated. This configuration permits Li/FeS_2 stack integration using a steel/steel weld. However, due to limitations in cell component sizing (as discussed later), an all Mo hardware battery, with bipolar seals in a ring/ceramic/ring configuration, was used in the assembly of the first 13 cm diameter bipolar Li/FeS_2 stack. The bipolar seal for Li/FeS stacks, using a steel ring/ceramic/steel ring configuration, is a much less challenging development. Coated steel may substitute for molybdenum in Li/FeS_2 batteries. Such seal configurations would permit easy bipolar stack integration using a steel-steel peripheral weld.

6.0 BIPOLAR BATTERY DEVELOPMENT AND TESTING

The purpose of cell testing is to evaluate the status of cell performance (e.g., specific energy and power) and cell stability (i.e., cycle life and capacity retention). For Li/FeS_2 cells, the most common testing consists of constant-current discharge (25 - 200 mA cm^{-2}) to a voltage cutoff (1.3 to 1.1 V) and constant current charge (25-50 mA cm^{-2}) to a voltage cutoff (2.05-2.15 V). A charging profile is being developed to equalize cell capacities in series connected batteries by trickle charging at 2-5 mA cm^{-2}. Computer simulated EV driving schedules (e.g., SFUDS) are conducted as a means of more accurately projecting cell performance under vehicle driving conditions. Bipolar cells and stacks are placed into a test fixture with movable platens that can be used to evaluate the effect of compressive load upon stack performance, via a pneumatic cylinder.

Another important area of the testing program has been post-test analyses. Extensive metallographic, analytical chemistry, and scanning electron microscopy analysis has provided valuable insight into cell degradation. In the earlier work on prismatic cells, mechanical defects contributed to cell short circuiting. Generally, these phenomena have been eliminated in the bipolar hardware.

Sealed and unsealed prototype bipolar lithium/sulfide cells have been tested. These bipolar cells are 7 mm thick, possess 13 cm diameter electrodes, and have a total weight of 0.25 kg (including the weight of two full current collectors). The electrode materials account for 48% of the total bipolar cell weight. The cell thickness breakdown is as follows: iron sulfide electrode, 2.2 mm; MgO powder separator, 1.8 mm; Li-alloy electrode, 3.0 mm. The separator is thicker than desired to aid handling of the 13 cm diameter pressed powder pellets. Electrodes and separator pellets were pressed at SAFT-America (Cockeysville, MD) using a 400 ton press. The 13 cm diameter pellets possess good handling properties. Future prototype bipolar cells will increase the thickness of the electrodes and reduce the thickness of the separator layer. This should further increase specific energy and power.

These first 13 cm diameter bipolar cells exhibit approximately 30% increased specific energy and more than double the specific power of earlier monopolar (prismatic design) cells. Li/FeS_2 bipolar cells are operated at 425°C using the LiCl-rich LiCl-LiBr-KBr electrolyte. The Li-alloy electrode consists of LiAl + LiAlFe to provide overcharge tolerance. Overcharge tolerance rates were measured at over 2.5 mA cm^{-2}. As shown in Fig. 13, both cell types deliver about 25 Ah at a 5 A discharge rate. These capacities translate to about 90% utilization for the U.P. FeS_2, electrode capacity and 70% utilization for the FeS electrode capacity. These values are similar to those obtained with 3 cm diameter bipolar cells.

The scale-up from 3 to 13 cm led to performance enhancement. The bipolar Li/FeS_2 cell delivers a specific energy of 180 Wh kg^{-1} at a 30 W kg^{-1} discharge rate, while the Li/FeS cell delivers 130 Wh kg^{-1} at a 25 W kg^{-1} discharge rate. The bipolar cell scale-up also yielded improved specific power as a result of lower internal impedance. Generally, it was more difficult to achieve uniform surface contact in the 3-cm diameter bipolar cells. Cell impedance was measured by a current interrupt method, with voltage relaxation recorded from milliseconds to about 15 s. This method indicates electronic and ionic contributions to cell impedance. Superior specific power was achieved for the bipolar Li/FeS_2 cell because of its high average discharge voltage and impedance stability throughout the discharge. As shown in Fig. 14, this first prototype cell had an impedance of 0.5 to 0.6 ohm cm^2 at 80% DOD. This indicates a peak specific power in excess of 400 W kg^{-1}.

A number of 13 cm diameter sealed bipolar Li/FeS_2 cells underwent post-operative metallographic analysis. The metallographic findings support the chemical/physical stability of our seal technology. In general there was no indication of electrolyte escape from the sealed bipolar cells. Also, unlike earlier prismatic ("monopolar") cells, the electrode and separator layers retained their "as fabricated" thicknesses, to within 10%. The bipolar seal assembly and processing methods continue to be refined.

A number of sealed Li/FeS_2 bipolar stacks (Fig. 1), employing four 13 cm diameter cells each, have been fabricated to evaluate stack performance and improve battery assembly techniques. The Li/FeS_2 bipolar stacks, having all Mo hardware, were assembled and placed on test recently. Aside from deficiencies in component sizing, especially an undersized separator, future stack assembly must accommodate some reduction in electrode thickness from the as-fabricated state. The stack assembly was accomplished by spot-welding the seal/bipolar plate/seal combination at the cell periphery. All four cells were integrated into the stack using a Tungsten Inert Gas (TIG) weld of the peripheral metal junctions. These bipolar stacks have achieved about 90% of cell performance; these first stacks are being operated with cell-level voltage cut-offs. These stacks have been operated 200-400 cycles.

As background, tests of overcharge-tolerant prismatic FeS_2 cells (25-Ah capacity) with reference electrodes (Ni/Ni_3S_2) have verified that the lithium-shuttle mechanism provides sufficient levels of overcharge tolerance. Such cells have operated over 200 cycles with high performance and stable overcharge tolerance. In Figure 15, the electrode potentials vs. percent of capacity utilization for a U.P. FeS_2 cell [Li-Al + 10 % $Li_5Al_5Fe_2$/LiCl-LiBr-KBr(MgO)/FeS_2] are given for a charge-discharge cycle. A bulk charge at 25 mA cm^{-2} to 2.03 V was followed by a trickle charge of 3.0 mA cm^{-2}. As seen in Fig. 15, the Li-alloy electrode undergoes about a 200 mV transition near full-charge capacity. This is crucial to ensure cell longevity. The U.P. FeS_2 electrode indicates negligible change in potential during the overcharge period; that is, it is protected from the deleterious effects of overcharge polarization. The self-discharge rate undergoes a stepwise increase to the trickle-charge rate. In this test, the trickle-charge period (8 h) charged 15% more coulombs into the electrode than the rated capacity, and the extended trickle charge did not contribute to additional capacity in the subsequent discharge.

Overdischarge of FeS_2 electrode is avoided by building lithium limited cells. When the Li-Al electrode is discharged into the α phase, a marked stepwise reduction in cell voltage occurs, indicating the end of discharge. The capacity of the Li-Al electrode is limited, as compared to that of the FeS_2 electrode to prevent appreciable formation of low-density Li_2S in the FeS_2 electrode

(a discharge reaction product that can negatively affect on cycle life if allowed to form in sufficient quantity). Typically this is accomplished by designing cells for 90% utilization of the U.P. FeS_2 capacity and 80% utilization of the Li-Al electrode. A cell of this type operated at over 98% coulombic efficiency for more 900 cycles, when the Li-Al electrode was allowed to polarize by ≥300 mV at the end of discharge [6].

The overcharge capacity safeguards the cell and permits unmonitored bulk charge at 30-60 mA/cm^2 with a battery voltage limit. A battery can thus be charged with a voltage that is 2.00 V multiplied by the number of cells in the battery (e.g., a 100-cell battery would be charged at 200 V). Assuming a bell-shaped distribution in charge capacity acceptance of cells at completion of a bulk charge, the "stronger" half of the battery cells would attain the overcharge capacity state. (The conventional electronic charger/equalizer, which monitors the voltage of each cell, would have ended the bulk charge when the first cell attained a charge cutoff voltage of 2.00 V). After the bulk charge, battery cell equalization is accomplished by a battery trickle charge of about 2.5 mA/cm^2. The "stronger cells, which have been safeguarded by the overcharge capacity, are charged at approximately 0% coulombic efficiency because the trickle-charge rate balances the lithium shuttle rate. The "weaker" cells, on the other hand, accept additional capacity at about a 2.5 mA/cm^2 rate over a 3-6 h period and undergo an additional 5-10% increase in capacity. The battery is effectively charge equalized when all the battery cells have reached the overcharge capacity state (without any electronic monitoring). Figure 12 provides the voltage/time plots of a small battery (four overcharge-tolerant cells connected in series) which has been operated to a battery voltage cutoff. A subsequent charge includes a trickle charge period near full-charge state. As a result of the lithium shuttle mechanism, the battery capacity has been increased, the strongest cell has not been jeopardized by overcharge, and weakest cell has increased in capacity.

7.0 SUMMARY AND CONCLUSIONS

It is worth noting that the R&D emphasis was only recently shifted away from prismatic Li-Al/FeS batteries to bipolar Li-Al/FeS and Li-Al/FeS_2 batteries with the main emphasis directed at bipolar Li-Al/FeS_2 batteries. Several major technical advances, achieved during the 1986-1990 time frame, inspired this shift to bipolar batteries. These major advances are summarized in Table 4.

The first technical advance deals specifically with the achievement of a more reversible FeS_2 cathode, based on the use of a low-temperature electrolyte and a dense cathode that is operated only on the upper voltage plateau. Acceptable reversibility has been demonstrated over 1000 cycles. The other three advances apply to both Li-Al/FeS_2 and Li-Al/FeS cells and batteries. Development of overcharge tolerance[25], in 1988, permitted consideration of bipolar stack designs, because an *in situ* means of balancing long strings of series connected cells is an essential ingredient for serious consideration of bipolar battery configurations. Development of the lithium rich electrolyte formulation, in 1989, helped reduce the weight and volume of electrolyte required in each cell, by permitting the change to electrolyte starved cells without sacrificing power[36]. Higher power and energy densities resulted from reducing weight and volume while maintaining similar power and energy. Also, electrolyte starved configurations are desirable in bipolar battery designs, where electrolyte containment is critical. Development of the first seal material in 1990, made bipolar battery designs practical for this technology[38]. This seal technology was demonstrated in 3 cm diameter laboratory cells, initially, and then scaled to 13 cm diameter EV

cells[34]. Further validation has been gained through the building and testing of several four cell stacks.

Table 4. Major technical advances in the development of bipolar lithium/iron sulfide cells

Time Frame (Year)	Major Technical Advance	Practical Implication
1986	Low-temperature electrolyte and upper-plateau dense FeS_2 cathode	Achieves > 1000 cycles
1988	Electrochemical overcharge tolerance	Makes bipolar design viable
1989	Li-rich electrolyte in starved cell	Enhances performance
1990	Sulfide ceramic seal material	Makes bipolar design practical

The projections of Fig.16 illustrate the magnitude of the performance enhancements associated with the use of the bipolar design. These performance projections[39] were developed as part of the design trade-off studies which the spread sheet model accounts for all the components and subsystems required to produce a fully operational EV battery, Fig. 17. Alternative battery designs are represented by dots, corresponding to an energy density from a battery designed to meet the acceleration power (expressed as power density) for the mission. Performance envelopes are, shown surrounding the design points for each basic design concept Also, Fig. 16 incorporates the mid-term and long-term performance objectives of the U.S. Advanced Battery Consortium (USABC), as well as typical performance requirements for three electric and hybrid vehicle applications (squares). The commuter vehicle considered here is a high-performance vehicle, similar to the GM Impact, that targets a 50% greater range capability than that achievable with lead-acid batteries.

Bipolar lithium sulfide batteries possess a number of very attractive attributes for EV applications, over and above their high-performance characteristics. These attributes include:

- Stable and reversible electrodes possess long-life capability;
- solid reactants, coated with electrolyte, provide inherent safety;
- *in situ* short circuiting of failed cells produces inherent battery stack reliability;
- inherent low impedance provides high power and rapid recharge capabilities;
- cells are tolerant to overcharge, overdischarge, and freeze/thaw abuse;
- Easy modification of electrode thickness provides a high degree of design flexibility and to achieve optimal performance in many vehicle applications;
- Bipolar stack simultaneously achieves high power and high energy.

The features of bipolar lithium iron sulfide batteries that produce these attractive attributes have been discussed in the body of this review. At this stage in the development of bipolar

The features of bipolar lithium iron sulfide batteries that produce these attractive attributes have been discussed in the body of this review. At this stage in the development of bipolar lithium iron sulfide batteries, they appear to be excellent candidates for a wide range of electric and hybrid vehicle applications.

Efficient production of base materials, lithium-alloys and lithium-salts (Sections 2.0 and 3.0), are critical to the commercial success of high temperature Li/FeS_2 batteries for electric cars. These lithium containing materials may account for about 50% of the battery materials costs. Molten-salt electrochemical research seeks to optimize utilization of the lithium capacity of lithium-alloy electrodes. Molten-salt electrolyte compositions have significantly enhanced the utilization and power capability of the iron disulfide electrode. Further advances in bipolar Li/FeS_2 battery performance have resulted from discovery and application of lithium-compatible ceramic materials. As in Section 4.0, sulfide ceramic sealants have enabled a large-diameter, metal/ceramic peripheral seal. As a consequence, the weight and volume fraction of cell hardware have been reduced by at least 50%. The bipolar design also aids the battery electrochemistry with more uniform current distribution for electrodes. Development of thin, tough ceramic separators can improve battery power, without reducing specific energy. Porous, rigid ceramic plates (eg. AlN) are prospective separators. Enhanced battery performance is a chief approach to more efficient use of battery materials.

ACKNOWLEDGMENTS

The authors gratefully acknowledge the support and encouragement rendered by K. M. Myles and C. C. Christianson. Cold pressed electrode and separator/electrolyte pellets for 13 cm diameter cells were supplied to ANL's specification by SAFT-America, Cockeysville, Maryland. This work was supported by the U.S. Department of Energy, K. Heitner and A. Landgrebe, project managers , and the State of Illinois.

REFERENCES

1. T. D. Kaun, P. A. Nelson, L. Redey, D. R. Vissers, G. L. Henriksen, "High Temperature Lithium/Sulfide Batteries, Electrochemical Acta 38,(9), 1269-1287 (1993).

2. T. D. Kaun, *J. Electrochem. Soc.* **132**, 3063 (1985).

3. T. D. Kaun, in *Proceedings of Joint International Symposium on Molten Salts*, Electrochemical Society, New Jersey, Vol. 87-7, p. 621. (1987).

4. D. A. Bruggerman, *Ann. Physik.* **24**, 636 (1935).

5. T. D. Kaun in *Proceedings of International Workshop on High-Temperature Batteries*, April 16, 1986, Argonne National Laboratory Report ANL-86-40, p. B-101 (1986).

6. T. D. Kaun, T. F. Holifield, and W. H. DeLuca, in *Proceedings of the Materials and Processes Symposium*, Eds., by K. M. Adams and B. B. Owens, Electrochemical Society, New Jersey Vol. 89-4, p. 383 (1989).

7. S. K. Preto, Z. Tomczuk, and M. F. Roche, Abstract 336, *Extended Abstracts,* Electrochemical Society, Vol. 130, p. 264 (1983).

8. J. A. Schmidt and W. Weppner, Abstract 344, *Extended Abstracts,* Electrochemical Society., Vol. 82-1, (1982).

9. T. Kaun, in *Proceedings of 21st Intersociety Energy Conversion Engineering Conference,* San Diego, California, p. 1043 (1986).

10. S. K. Preto, Z. Tomczuk, S. von Winbush, and M. F. Roche, *J. Electrochem.* Soc. **130,** 264 (1983).

11. T. D. Kaun, in *Proceedings of the Symposium on Rechargeable Lithium Batteries,* Ed., S. Subbaro, Electrochemical Society, New Jersey, Vol. 90-5, p. 274 (1990).

12. C. J. Wen, B. A. Boukamp, R. A. Huggins, and W. Weppner, *J. Electrochem. Soc.* **126,** 2258 (1979).

13. K. M. Myles, F. C. Mrazek, J. A. Smaga, and J. Settle, in *Proceedings of Workshop on Advanced Battery Research Design,* Argonne National Laboratory Report ANL-76-8, p. 69 (1976).

14. T. D. Kaun and P. A. Nelson, *Lithium Transport in Molten-Salt Electrolyte Battery Cells Leading to Overcharge Tolerance,* presented at AIChE Meeting, Chicago, IL, November 11-16, 1990.

15. P. A. Nelson and T. D. Kaun, *Molten Salt Techniques,* Eds., by R. J. Gale and D. G. Lovering, Plenum Press, London, pp. 229-265 (1991).

16. C. J. Wen and R. A. Huggins, *J. Solid State Chem.* **37,** 271 (1981).

17. H. G. V. Schnering, R. Nesper, K. F. Tebbe, and J. Curda, *Z. Met* **71,** 357 (1980).

18. D. R. Vissers, Z. Tomczuk, L. Redey, and J. E. Battles, in *Lithium,* Ed. O. Bock, Chapter 10, Wiley, New York (1985).

19. T. D. Kaun, U. S. Patent No. 4,158,720 (1979).

20. G. E. Lagos, I. Purada, G. Crisostomo and J. Cervalan, Extended Abstracts, Electrochemical Society, New Orleans, LA, Vol. 93-2, p. 30 (1993).

21. T. D. Kaun and P. A. Nelson in Proceedings of "Lithium Batteries" Symposium Eds., N. Doddapanani and A. Landgrebe , Electrochemical Society, New Jersey, Vol. 94-4, pp. 63-74 (1994).

22. D. R. Vissers, L. Redey, and T. D. Kaun, J. Power Sources, 26, 37 (1989).

23. E. P. Van Artsdalen and G. Jaffe, J. Phys. Chem. **59,** 119 (1955).

24. L. Redey, J. Electrochem. Soc. **136,** (1989).

25. T. D. Kaun, T. F. Holifield, M. F. Nigohosian, and P. A. Nelson, in *Proceedings of the Materials and Processes Symposium,* Eds., K. M. Adams and B. B. Owens, Electrochemical Society, New Jersey, Vol. 89-4, p. 383 (1989).

26. J. Smaga, in *Proceedings of the International Workshop on High-Temperature Molten Salt Batteries,* Argonne National Laboratory Report ANL-86-40, pp. B72-B87 (1986).

27. J. A. Smaga, F. C. Mrazek, K. M. Myles, and J. E. Battles, in *Materials Requirement in LiAl/LiCl KCl/FeS.* Secondary Batteries, Eds. N.J. Hoffhian and G. A. Whitlow, National Association of Corrosion Engineers, Houston, TX pp. 52-64, (1978).

28. R. B. Swaroop, J. E. Battles, and R. S. Hamilton, in *Proceedings of the 6th Inter-American Conference on Materials Technology,* San Francisco, CA, pp. 67-71 (1980).

29. J. P. Mathers, C. W. Boquist and T. W. Olszanski, J. Electrochem Soc. **12,** 1913 (1978).

30. N. Shuster and H. N. Seiger, in *Proceedings of the 35th Power Sources Symposium,* Cherry Hill, New Jersey, P. 354 (1992).

31. J. E. Battles, J. A. Smaga, and K. M. Myles, Met. Trans. **9A** 183 (1978).

32. T. D. Kaun and J. A. Smaga, Bipolar Battery with Array of Sealed Cells, U.S. Patent No. 4,687,717. (1987).

33. T. D. Kaun, U. S. Patent #5,162,172 (1992).

34. T. D. Kaun, U. S. Patent 5,194,298 (1993).

35. T. D. Kaun, M. J. Duoba, K. R. Gille, and J. A. Smaga, in *Proceedings of the Symposium on Rechargable Lithium Batteries* Eds. by S. Subbaro, Electrochemical Society, New Jersey, Vol. 90-5, p. 315 (1990).

36. W. D. Kingery, H. K. Bowen, and D. R. Uhlmann, *Intro. to Ceramics,* Wiley and Sons, New York, p. 791 (1976).

37. T. D. Kaun, M. J. Duoba, W. Johli, V. Luong, F. Mrazek, D. Palkon and D. Simon, in *Proceedings of 26th Intesociety Energy Conversion Engineering Conference,* Boston, MA, Vol. 3, p. 417 (1991).

38. T. D. Kaun, M. J. Duoba, K. R. Gillie, D. R. Simon and D. R. Vissers, in *Proceedings of the 34th International Power Source Symposium,* Cherry Hill, New Jersey, p. 29 (1990).

39. P. A. Nelson and T. D. Kaun in *Proceedings of 26th Intersociety Energy Conversion Engineering Conference,* Boston, MA, Vol. 3, p.417 (1991).

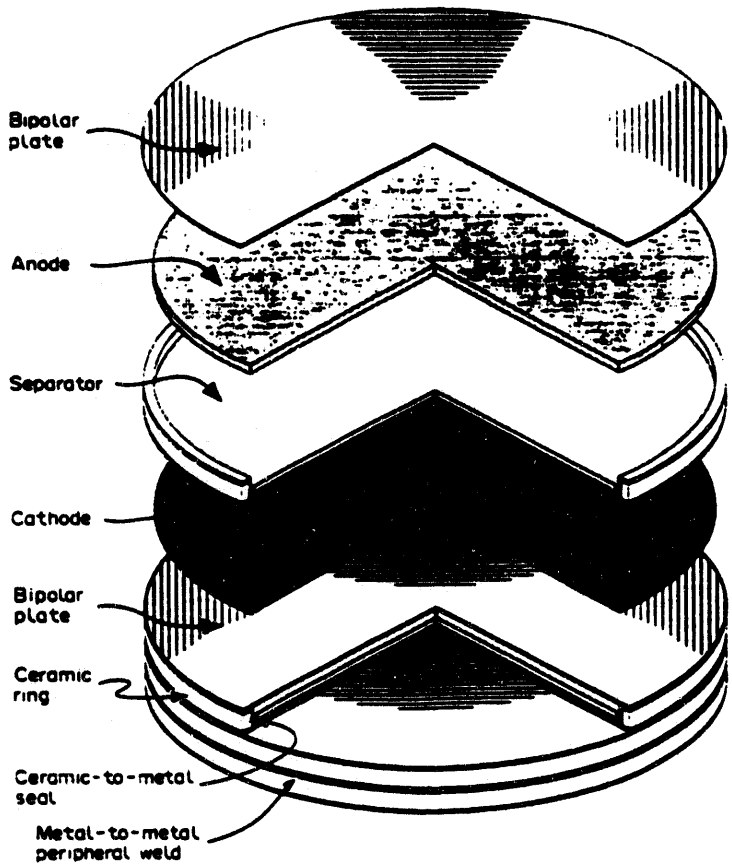

Fig. 1. Exploded View of Cell of a Four Cell Bipolar Stack. Final assembly involves a peripheral weld of the bipolar plate to the metal ring that is captured in the ceramic-to-metal seal.

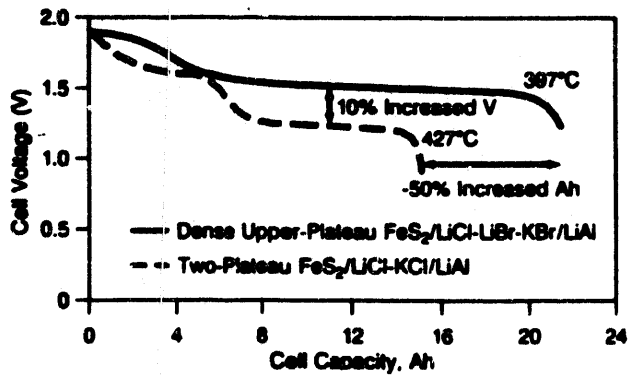

Fig. 2. Voltage/Capacity Curves at a Discharge Rate of 50 mA/cm². FeS_2 cell energy density improved by 75% and power doubled at 80% DOD for U.P. FeS_2 electrode as compared to two-plateau electrode cells of same volume and separator area [100 cm²].

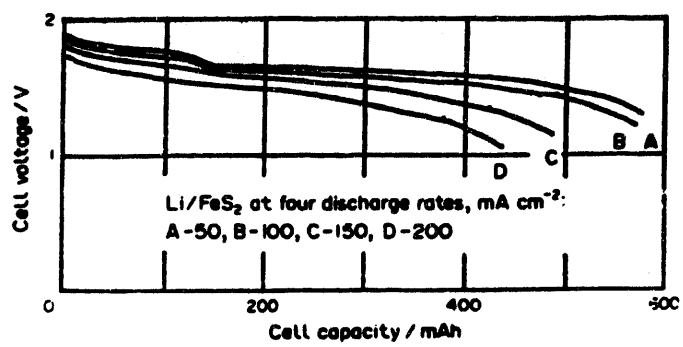

Fig. 3. Voltage/Capacity Plot of a Bipolar Li/FeS_2 Cell (5 cm² Area, 625 mAh Theoretical Capacity) Operated at 425°C.

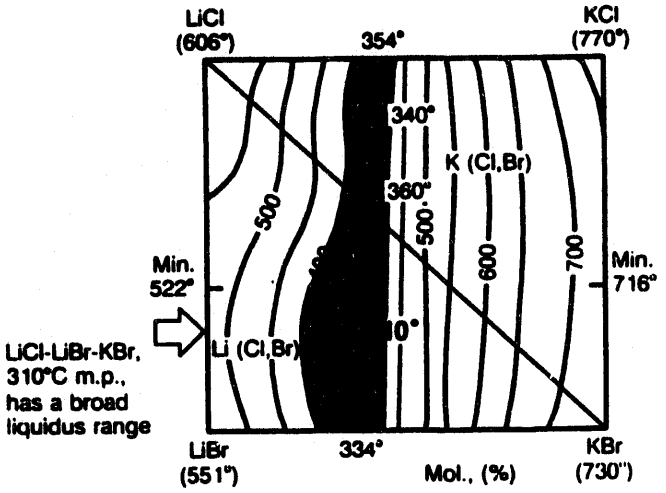

Fig. 4. Phase Diagram of LiCl-LiBr-KBr Molten-Salt.

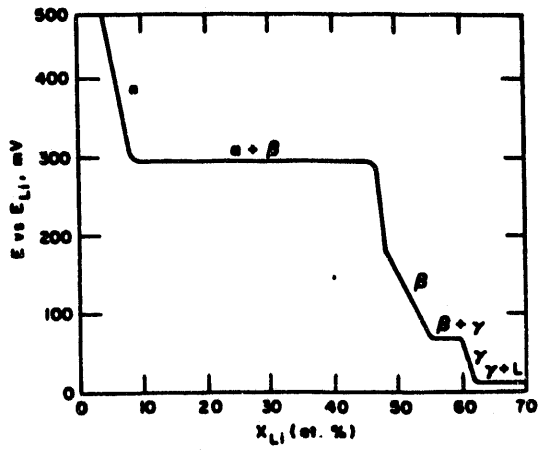

Fig. 5. Coulometric Titration Curve for Lithium-Aluminum System at 423°C.[12]

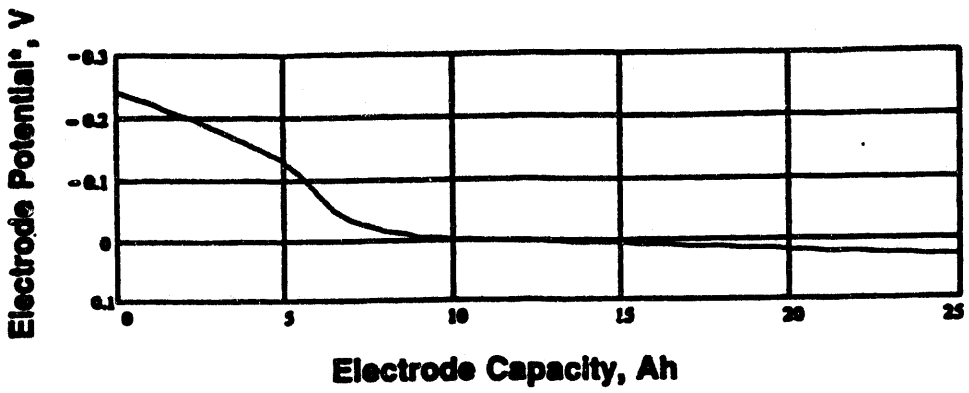

* Potential vs. LiAl Reference Electrode, 25 at%, Li-Al during charge half-cycle

Fig. 6. Electrode Potential vs. Charge Capacity of Two Phase Li-Alloy Electrode, 90% Li-Al + 10% $Li-Al_5Fe_2$ (25-Ah) in LiCl-LiBr-KBr at 425°C.

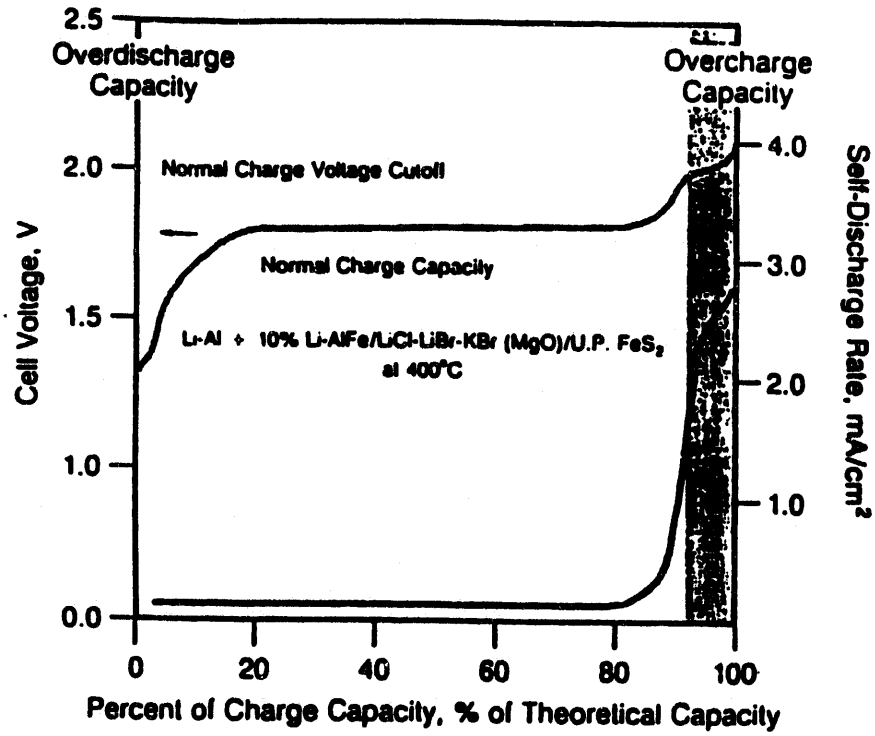

Fig. 7. Li/FeS_2 Cell Self-Discharge Rate as Related to State of Charge, LSM Rate Increased Due to Increased Lithium Electrode Activity in Overcharge Capacity.

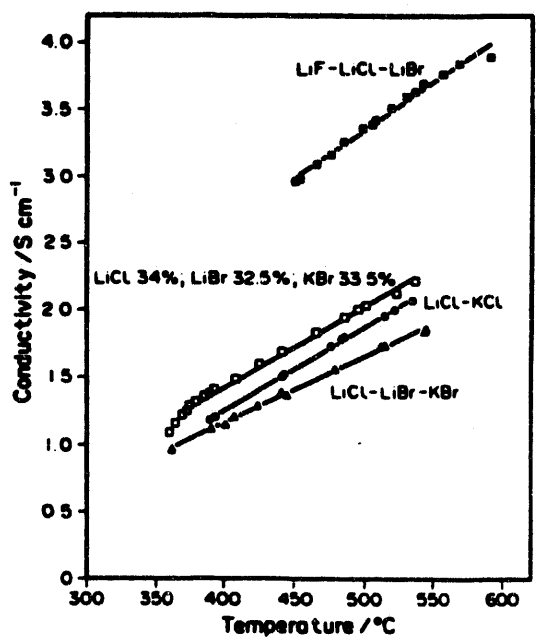

Fig. 8. Conductivities of Molten Salts for Rechargeable Lithium Batteries. The data for the three eutectic compositions are compared to a LiCl rich composition of LiCl-LiBr-KBr.

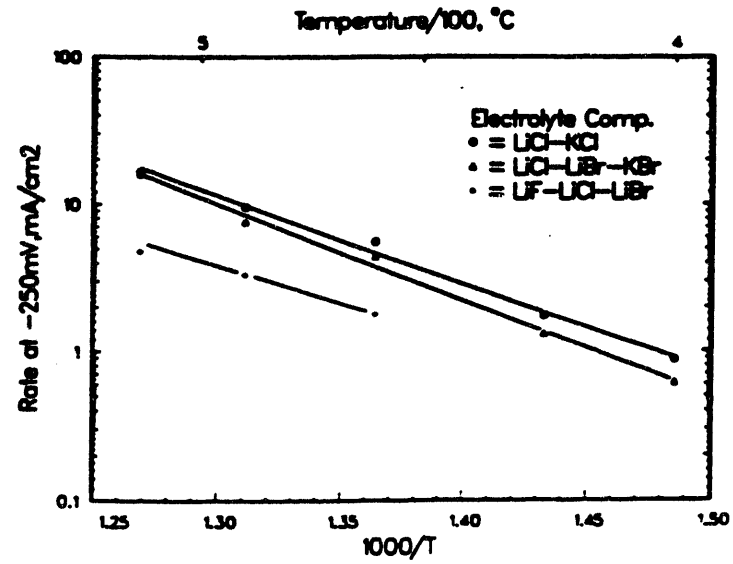

Fig. 9. Effect of Temperature Upon Lithium Shuttle Rates at about -250 mV vs. Li-Al Reference Electrode in Three Molten-Salt Electrolytes.

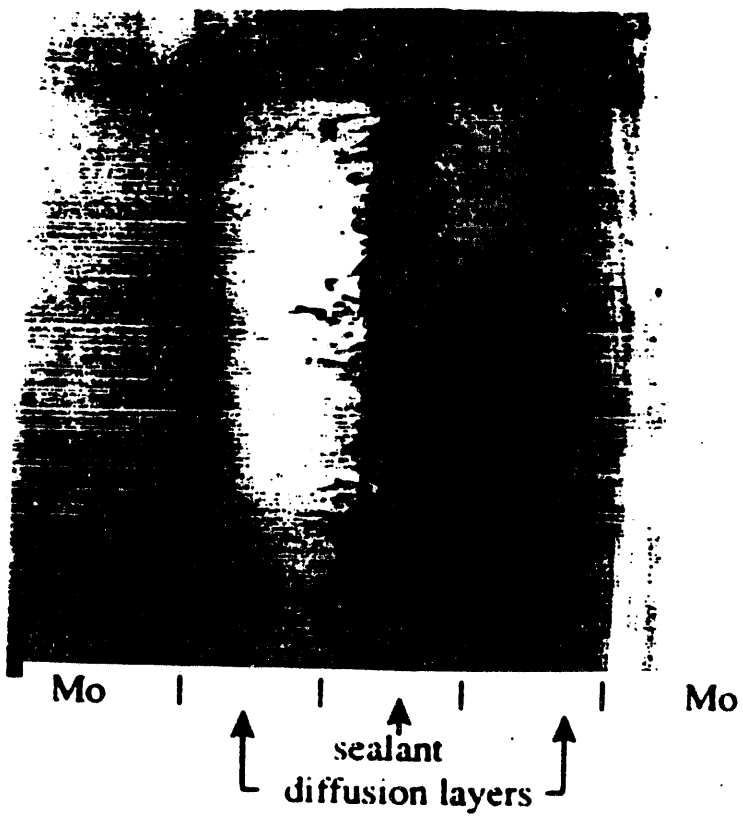

Fig. 10. Crossection (500 X) of Mo Bonded to Mo via Sulfide Ceramic Sealant.

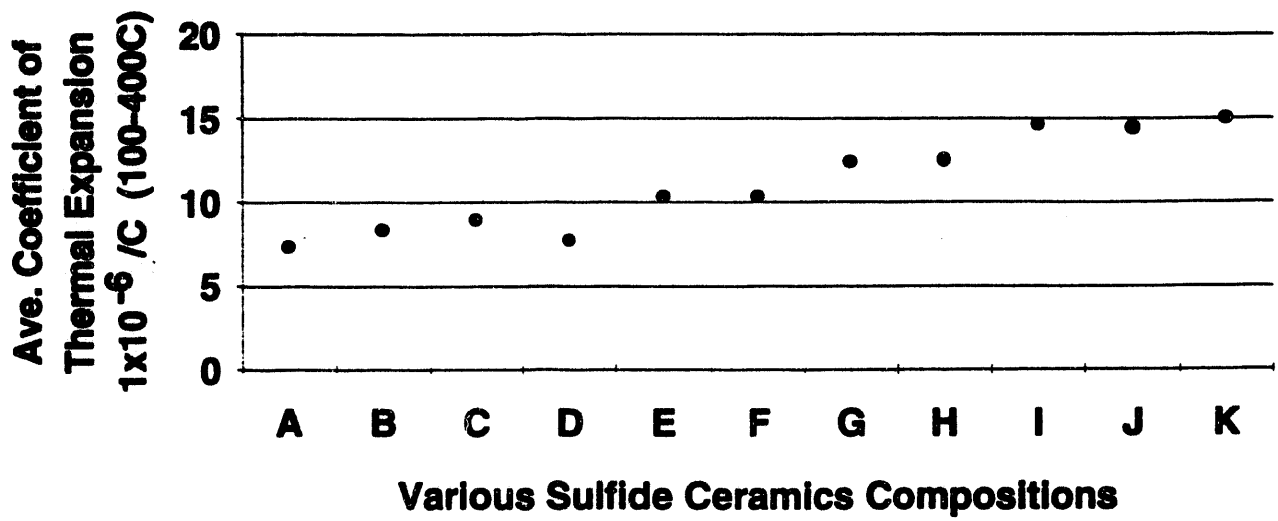

Fig. 11. Range of Coefficients of Thermal Expansion, CTE, Available from Sulfide Ceramics.

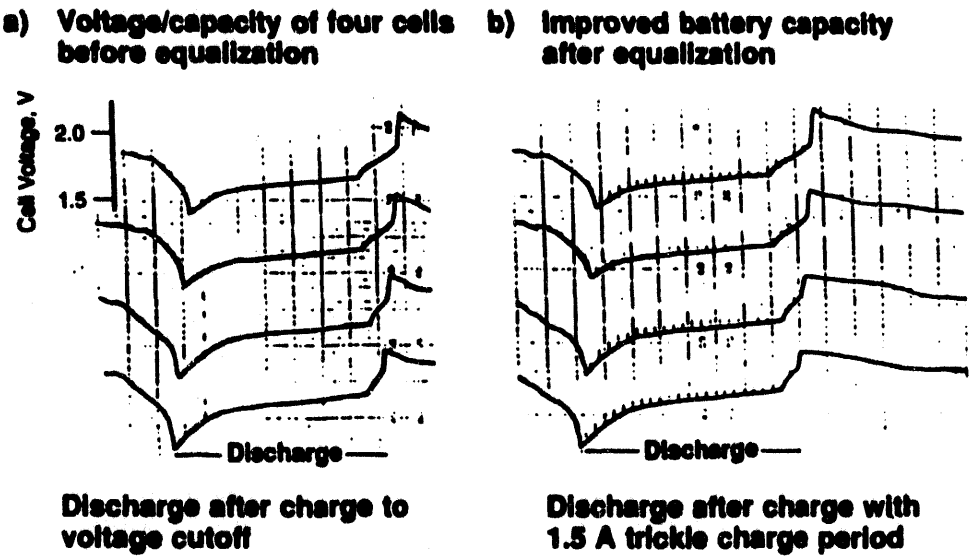

Fig. 12. Two Successive Voltage/Time Plots of a Four-Cell Li/FeS_2 Battery, Illustrating Battery Equalization by Trickle Charging the Battery.

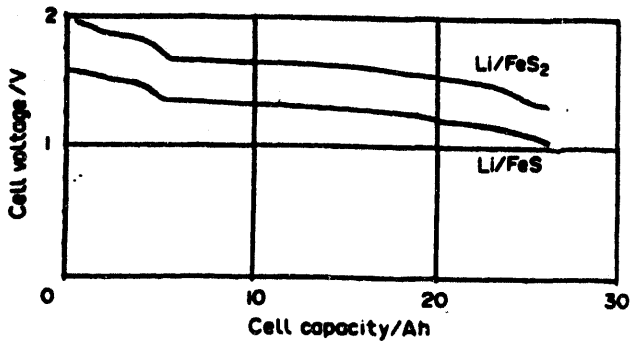

Fig. 13. Voltage/Capacity Plots of Prototype Bipolar Li/FeS_2 and Li/FeS cells at 425°C. Both cells weigh about 0.25 kg.

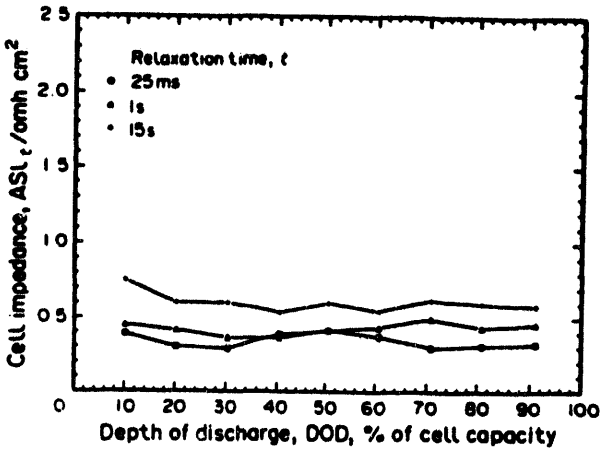

Fig. 14. Cell Impedance (ASI_t) vs. Depth of Discharge for Prototype Bipolar Li/FeS_2 Cell at 425°C.

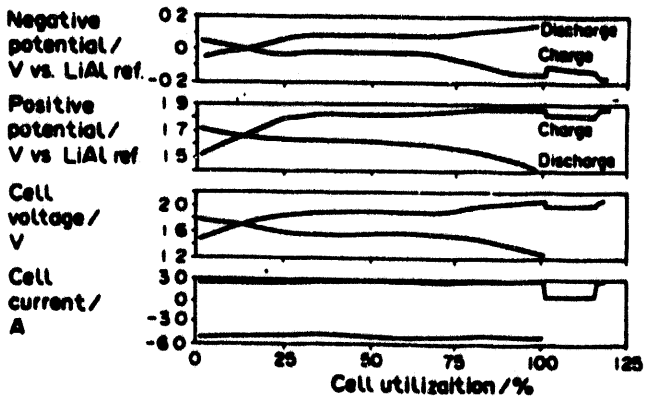

Fig. 15. Overcharge Tolerance of U.P. FeS_2 Cell Operated at 425°C and Over-charged by 15% at 3 mA cm^{-2}. No polarization of U.P. FeS_2 (positive) electrode indicates over-charge safeguard.

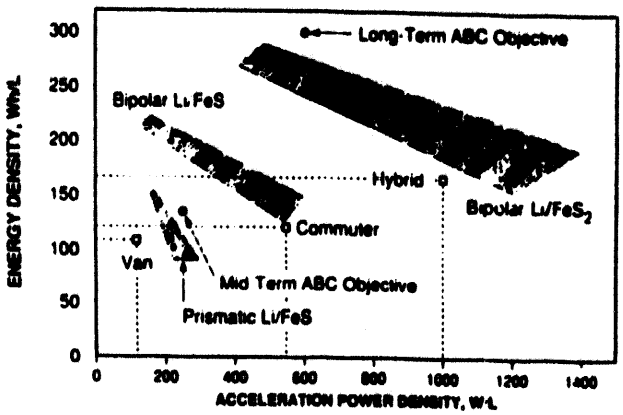

Fig. 16. Performance Projections for Lithium/Iron Sulfide Batteries. The dots in the performance bands are projections for battery designs from the design trade-off study. ABC stands for the U.S. Advanced Battery Consortium.

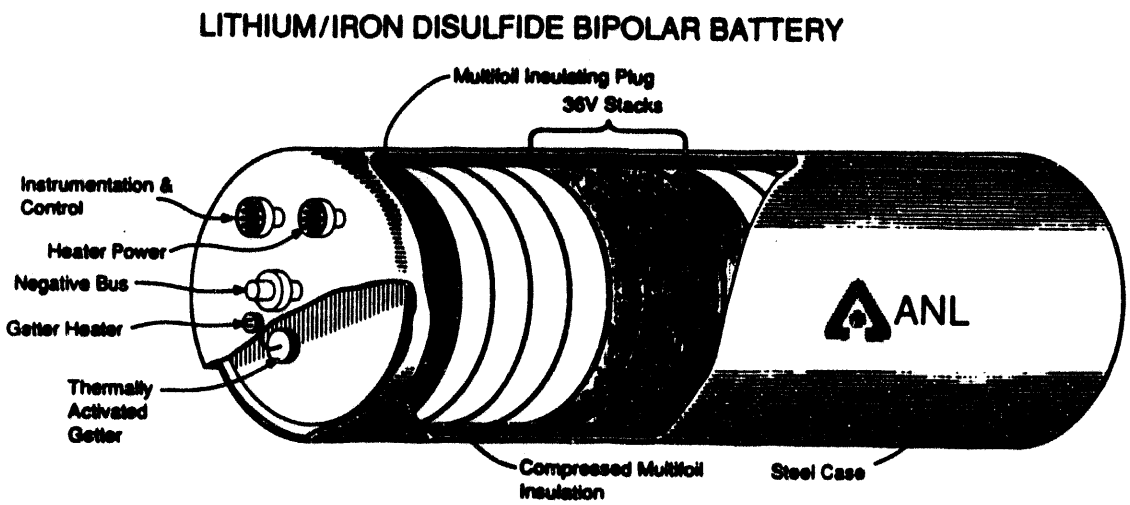

Fig. 17. Conceptual Design of Bipolar Lithium/Sulfide Battery Module Showing Vacuum Insulating Jacket and Compact Bipolar Construction.

DATE

FILMED

7/19/94

END